Available online at www.sciencedirect.com
ScienceDirect
Trans. Nonferrous Met. Soc. China 24(2014) 2251−2257
Transactions of Nonferrous Metals Society of China
www.tnmsc.cn

Effect of mechanical alloying and sintering process on microstructure and mechanical properties of Al−Ni−Y−Co−La alloy

Yan-bo YUAN[1], Zhi-wei WANG[1], Rui-xiao ZHENG[1], Xiao-ning HAO[1], Kei AMEYAMA[2], Chao-li MA[1]

1. Key Laboratory of Aerospace Advanced Materials and Performance of Ministry of Education, School of Materials Science and Engineering, Beihang University, Beijing 100191, China;
2. Department of Mechanical Engineering, Faculty of Science and Engineering, Ritsumeikan University, 1-1-1Nojihigashi, Kusatsu, Shiga 525-8577, Japan

Received 17 October 2013; accepted 30 April 2014

Abstract: $Al_{86}Ni_7Y_{4.5}Co_1La_{1.5}$ (mole fraction, %) alloy powder was produced by argon gas atomization process. After high-energy ball milling, the powder was consolidated by vacuum hot press sintering and spark plasma sintering (SPS) under different process conditions. The microstructure and morphology of the powder and consolidated bulk sample were examined by X-ray diffraction (XRD), scanning electron microscopy (SEM) and transmission electron microscopy (TEM). It is shown that amorphous phase appears when ball milling time is more than 100 h, and the bulk sample consolidated by SPS can maintain amorphous/nanocrystalline microstructure but has lower relative density. A compressive strength of 650 MPa of $Al_{86}Ni_7Y_{4.5}Co_1La_{1.5}$ nanostructured samples is achieved by vacuum hot extrusion (VHE).

Key words: mechanical alloying; aluminum alloy; nanocrystalline alloy; amorphous; spark plasma sintering; hot extrusion

1 Introduction

Recently, Al alloys containing rare earth (RE) and transition metal (TM) have attracted significant attention, because of their high strength and potential application in aerospace and automobile industry [1,2]. It has been reported that the strength of some Al−RE−TM alloys could be even further improved by partial crystallization and formation of uniformly distributed nano-scale FCC Al particles in the amorphous matrix [3−7]. However, the high strength of this level was only achieved in tensile tests of small pieces of ribbon samples, because amorphous or amorphous/nanocrystalline microstructures could be obtained only by the melt-spinning technique due to the lack of sufficient glass forming ability in the Al−RE−TM systems [8,9]. An alternative way of preparing amorphous materials is solid state reaction, for example, mechanical alloying (MA) of elemental powder and consolidation of amorphous powder material by extrusion or sintering techniques [10]. This technology has attracted growing interests [11−14] for the production of bulk glassy samples with large dimensions and complex shapes.

In this work, partial amorphous Al−Ni−Y−Co−La powder was attempted to synthesis by high-energy ball milling with appropriate adjustment of milling conditions, and the amorphous Al−Ni−Y−Co−La powder was consolidated by SPS and vacuum hot extrusion (VHE) to produce ultrahigh strength bulk Al-based amorphous/nanocrystalline composites. The microstructure was examined by TEM and XRD. The mechanical properties of the consolidated bulk samples were evaluated by the compression tests. The results were discussed based on detailed microstructural characterization in order to explore the possibility of producing ultrahigh strength aluminum-based alloys.

2 Experimental

$Al_{86}Ni_7Y_{4.5}Co_1La_{1.5}$ (mole fraction, %) alloy was prepared by Al, Ni, Y, Co and La with purities of 99.9%.

Foundation item: Project (2012CB619503) supported by the National Basic Research Program of China; Project (2013AA031001) supported by the National High Technology Research and Development Program of China; Project (2012DFA50630) supported by the International Science & Technology Cooperation Program of China
Corresponding author: Chao-li Ma; Tel: +86-10-82339772; E-mail: clma2001@gmail.com
DOI: 10.1016/S1003-6326(14)63341-0

These raw materials were melted together in a vacuum induction furnace under argon atmosphere. The powder of the alloy was produced by ultrasonic atomization, with the size range from 5 nm to 40 mm. Ball milling was carried out in a planetary high energy ball mill (XQM-2L) at room temperature using stainless steel vials and balls as milling media and alcohol as process controlling agent (PCA). The milling speed was from150 to 375 r/min, and ball-to-powder ratio was from 10:1 to 20:1, respectively.

The atomized $Al_{86}Ni_7Y_{4.5}Co_1La_{1.5}$ powder was consolidated by CIP and VHE. Powder was extruded to fully dense bars of 10 mm in diameter and 100 mm in thickness using high strength heat-resistant stainless steel punches and die. The VHE was carried out under a vacuum of 5×10^{-3} Pa for 30 min in the temperature range from 773 to 823 K (heating rate of 25 K/min). Before sintering temperature was arrived, the powder was degassed at 673 K for 1 h. The uniaxial pressure was applied to the powder mass throughout the VHE cycle.

Then the atomized $Al_{86}Ni_7Y_{4.5}Co_1La_{1.5}$ powder was consolidated using a SPS machine (Sumitomo Coal Mining Model 1050). 2 g powder was placed into a graphite die with 10 mm in diameter and sintered under vacuum at 4.0×10^{-3} Pa for 10 min at 773 K.

Phase identification was performed by RIGAKU RINT-2000 X-ray diffractometer with Cu K_α radiation and image plate detector over the 2θ range of 20°−90° at 0.02° step size. CamScan-3400 was used to observe the particle morphology and microstructure of the powder. TEM observations were performed on JEM-2100F instrument. The mechanical properties of the sintered samples were evaluated by the compression test using cylindrical specimens with d3 mm × 6 mm.

3 Results and discussion

3.1 Microstructure of mechanically alloyed powder

The SEM images show the initial aluminum alloy powder with particle size of 15 μm, however, the particle size of powder milled for 40, 100 and 160 h are about 13, 9 and 5 μm, respectively. This indicates the crystalline grain is steadily refined with the increase of milling time due to the continued impact of grinding spheres. Figure 1 shows that the starting powder is nearly smooth sphere while the powder milled for 40, 100 and 160 h has a amount of layer shape, which is caused by the sphere particle of starting powder getting squashed and fractured by the fragmentation of fragile flakes and/or by a fatigue failure mechanism with collision of steel spheres. Further milling results in severe plastic deformation of clusters and further reduction in particle size.

Figure 2 shows the XRD patterns of $Al_{86}Ni_7Y_{4.5}Co_1La_{1.5}$ alloy powder milled for 40 and 100 h. For the

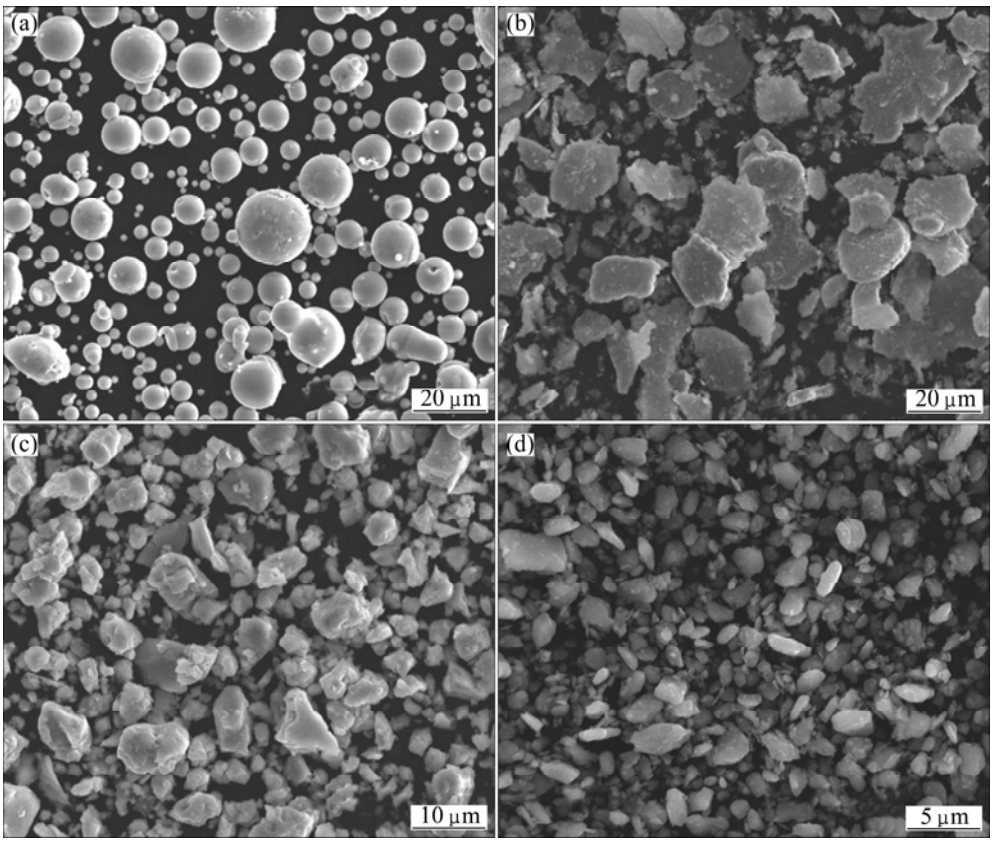

Fig. 1 SEM images of as-atomized $Al_{86}Ni_7Y_{4.5}Co_1La_{1.5}$ powder (a), powder milled for 60 h (b), powder milled for 100 h (c), and powder milled for 160 h (d)

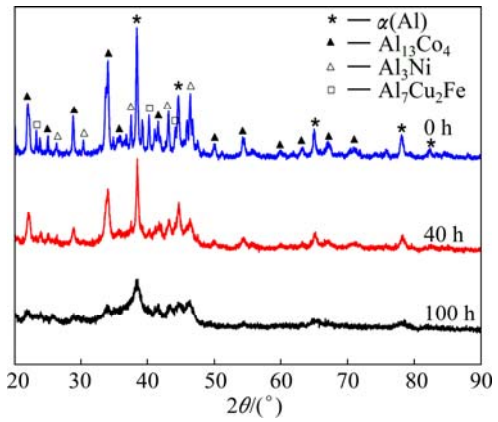

Fig. 2 XRD patterns of as-atomized powder and ball-milled powder of $Al_{86}Ni_7Y_{4.5}Co_1La_{1.5}$ for different time

as-atomized sample, intensive peaks of pure Al are detected together with some peaks stemming from intermetallic phases (Al_3Ni). After milling for 40 h and 100 h, only the most intensive peaks of pure α(Al) and $Al_{13}Co_4$ remain with a low intensity besides the halo peak. No distinct crystalline peaks can be found on the XRD pattern of the powder milled for 100 h, suggesting that the sample is amorphous within the resolution of XRD.

The SEM images of the as-atomized powder on cross-sections are shown in Fig. 3. The morphologies of the precipitates vary obviously with the changes of powder size and chemical compositions. For powder with a diameter size smaller than 25 μm, the precipitates are small and homogeneously distributed in matrix (Fig. 3(c)). While the size of the powders is larger than 50 μm, the precipitates become coarse, and present a needle shape (Fig. 3(b)). It should be noted that the size of $Al_{13}Co_4$ precipitated in the powder with a diameter more than 50 μm is 5−15 times larger than that in the small ones. As shown in Fig. 3(b), the strip like primary Al_3Ni phases (marked with circles) only exist in the powder with a diameter more than 50 μm, whereas the formation of the primary Al_3Ni is depressed in the small powders. Besides, powder (Fig. 3(d)) with a diameter less than 10 μm is amorphous.

The effect of size on the microstructures of the as-atomized powders can be explained by the cooling rate during atomizing process. It has been reported that the cooling rates vary from 102 to 104 K/s [15] with the different powder sizes, atomization pressures and thermal coefficients of the injection gas [16−18]. Generally, small powder possesses large specific surface areas, which is beneficial to the thermal conduction and rapid solidification. In the case of high cooling rate, the equilibrium microstructure transformation is

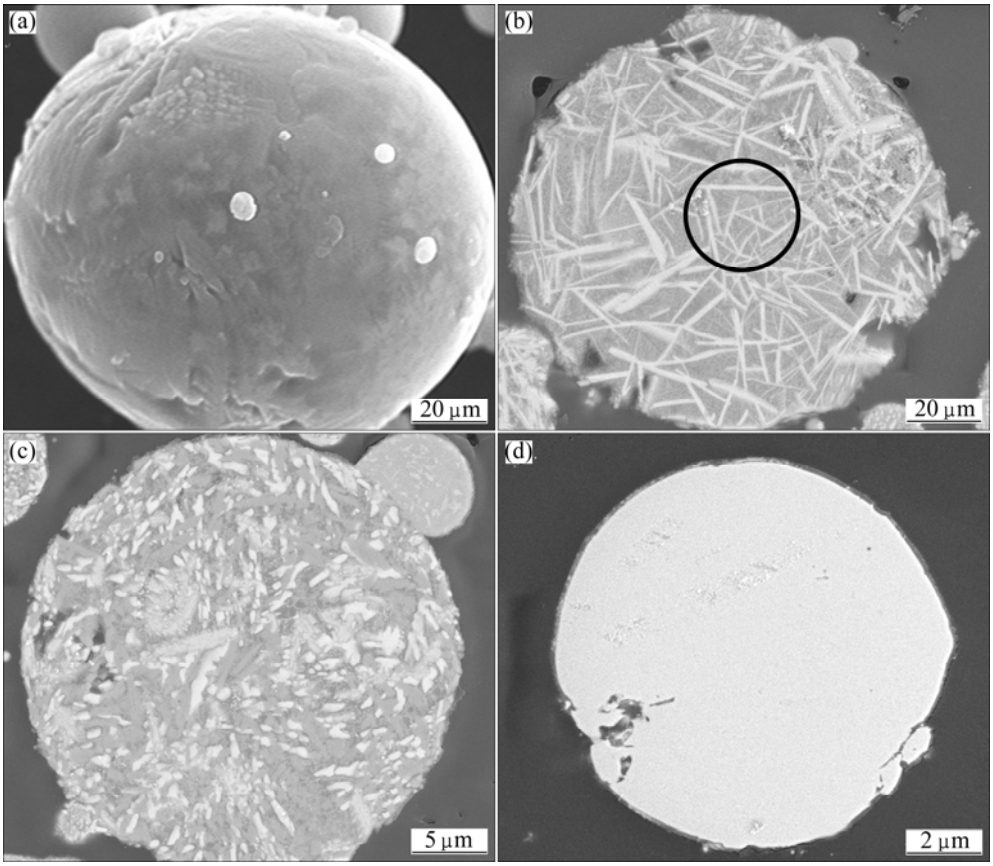

Fig. 3 SEM images of cross section of as-atomized $Al_{86}Ni_7Y_{4.5}Co_1La_{1.5}$ powder with different powder sizes: (a) 100 μm; (b) 50 μm; (c) 25 μm; (d) 5 μm

considerably decreased due to the higher degree of super-cooling and non-equilibrium thermodynamic conditions. More nuclei would be formed, and growth velocity would be decreased, which result in the fine Al_3Ni and $Al_{13}Co_4$ precipitates, as shown in Fig. 3(c). Under extremely rapid solidification condition, the primary phase would be completely restrained. This similar phenomenon also occurred in previously reported work [19]. Owing to the fine powder size (<25 μm) and helium solidification condition, the microstructure is only composed of the Al matrix supersaturated with Si, Ce and Ni. The formations of primary Al_3Ni and $Al_{11}Ce_3$ are completely restrained in as-atomized powder.

The other featureless particles surrounded by an amorphous/nanocrystalline matrix consist of α(Al) nanocrystals of about 10 nm in diameter. The nanocomposite particles are shown in Fig. 4.

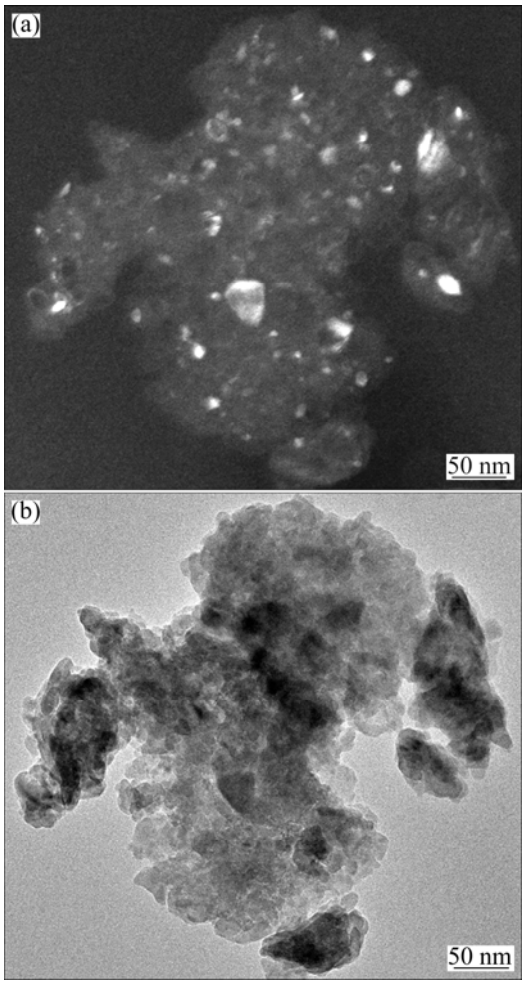

Fig. 4 Dark (a) and bright (b) field TEM images of powder milled for 48 h

3.2 Microstructure of sintered alloys

Figure 5 shows the back-scattered electron images (BEI) of the bulk sample sintered by VHE and SPS. The consolidated bulk sample has no pores (Fig. 5(a)), showing the attainment of full density. The powder boundaries can be clearly observed as a dark contrast. These dark regions were confirmed to be pure Al by EDS. Compared with Fig. 1(c), the particle does not deform obviously after extrusion. Because of quick elevating temperature and short holding time, the SPS bulk sample (Figs. 5(d)−(f)) maintains the original powder size well compared with VHE sample. However, the bulk sample sintered by SPS has lower relative density than VHE bulk sample, and many pores are also shown in Figs. 5(d)−(f). Besides, Figs. 5(e) and (f) also show that the size of the powder is larger than 50 μm, and the precipitates become coarse and present a needle shape, as shown in Fig. 3(b).

Figure 6(a) shows a bright-field TEM image of the VHE sample at 773 K after milled for 40 h with 5% (mass fraction) PCA. The microstructure is composed of a randomly oriented nanocrystalline grain region and coarse grains with size of 100 nm. During the consolidation process, the unusually high nucleation events result in the fact that the crystallized Al, Al_3Ni and $Al_{13}Co_4$ phases are homogeneously distributed. The diffraction spots in Fig. 6(c) correspond to $Al_{13}Co_4$ phase. The HRTEM shows that the boundary between matrix and intermetallic are semi-coherent. These indicate that the precipitate has good bonding with matrix.

Figure 7(a) shows a bright-field TEM image of the SPS sample at 773 K after milled for 100 h with 5% PCA. This bulk sample also maintains the morphology of original powder well. The amorphous phases shown in Fig. 7(c) prove that powder metallurgy can make amorphous/ nanocrystalline bulk alloy. Some order and disorder arrays in HRTEM image prove the existence of nanocrystalline in amorphous matrix. It has been demonstrated that this microstructure can attain super high strength.

Figure 8 shows the room temperature compressive engineering stress−strain curves of the extruded sample sintered by VHE produced from the powder milled for 48 h. The pure $Al_{86}Ni_7Y_{4.5}Co_1La_{1.5}$ alloy is too brittle to make compressive experiment, so 2024 Al alloy powder and original powder are blent, and strength is changed by adjust the component of original powder. The results show that the strength descends with the increasing component of 2024 Al alloy. In addition, sintering temperature is altered to attain high strength and high ductility. The compression strength is almost 650 MPa. The excellent compression strength is attributed to the fine grain size and the tiny and dispersed particles (Al_3Ni and $Al_{13}Co_4$). However, the experimental results above are still insufficient, and additional XRD, TEM and micro-hardness studies are presently underway to illustrate the strengthen mechanism of the extruded sample.

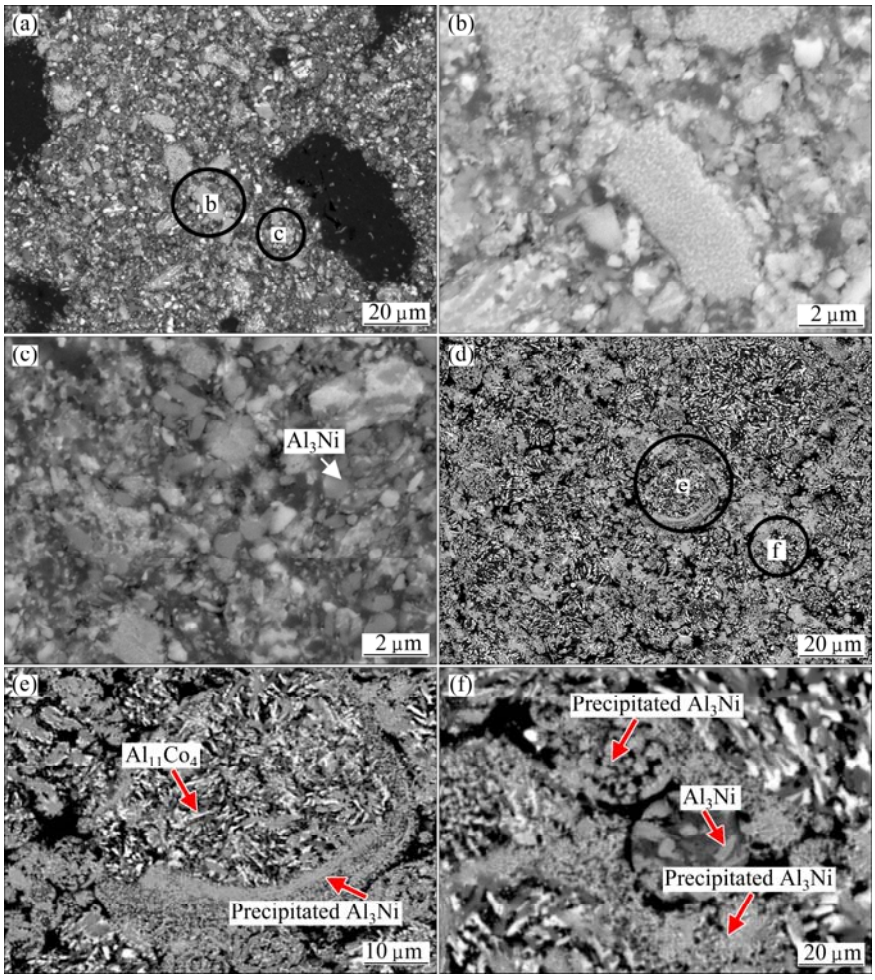

Fig. 5 SEM image of VHE alloys (a) and magnification images of region surrounded by circle (b, c), BEI image of SPS alloys (d) and magnification image of region surrounded by circle (e, f)

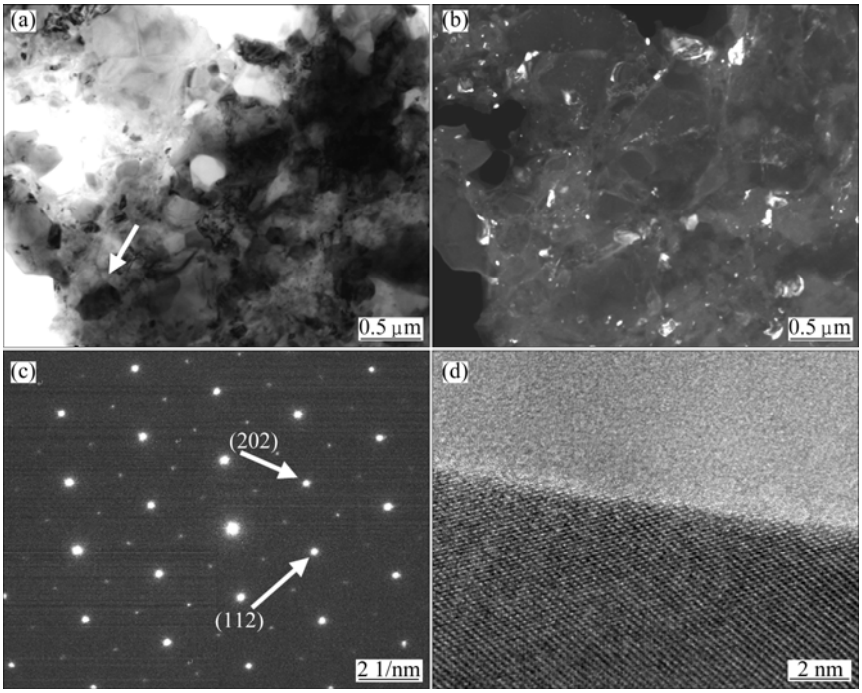

Fig. 6 TEM images of alloy after VHE: (a) Bright-field TEM image; (b) Dark-field TEM image; (c) Micro-beam diffraction pattern obtained from a particle indicated by an arrow in (a); (d) HRTEM image of boundary between matrix and intermetallic

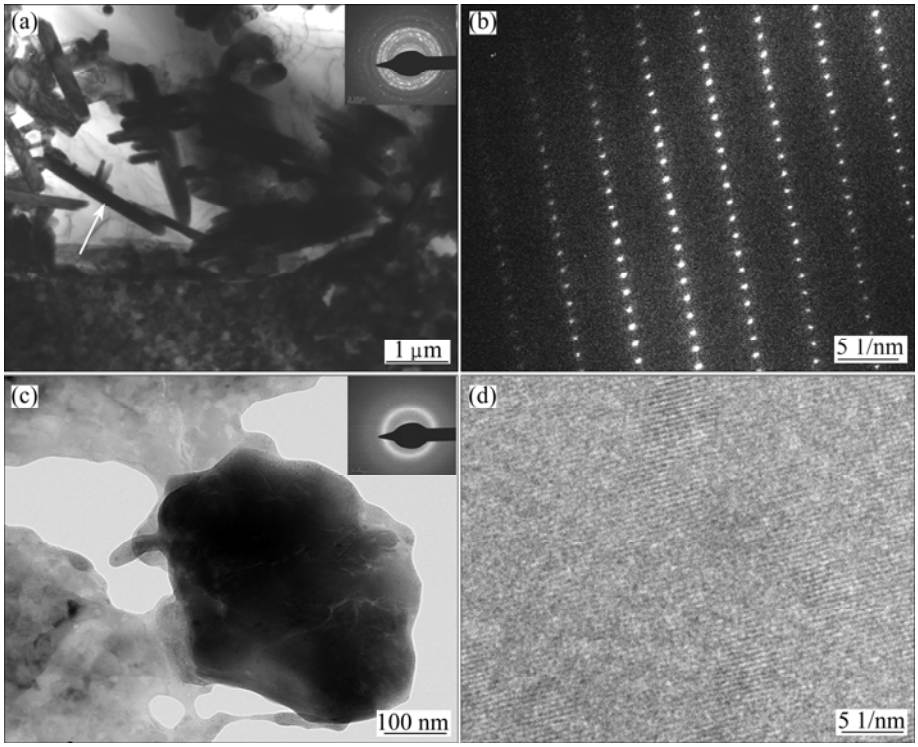

Fig. 7 TEM images of alloy after SPS: (a) Bright-field TEM image; (b) Micro-beam diffraction pattern obtained from particle indicated by arrow in (a); (c) Bright-field TEM image of amorphous phases; (d) HRTEM image

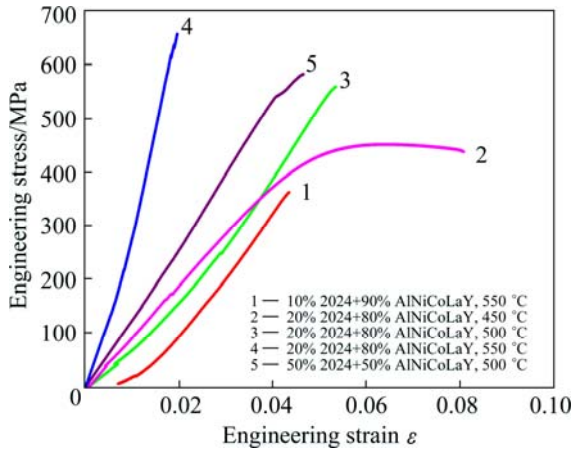

Fig. 8 Compressive engineering stress−strain curves of VHE samples

4 Conclusions

1) Experiments have been given on amorphization of the Al-based alloys by mechanical milling, however, amorphization needs certain condition such as exceeding 100 h ball milling and some starting materials like amorphous ribbons.

2) Amorphous/nanocrystalline bulk alloy can be prepared by SPS, but high relative density bulk alloy can not be obtained by this technique.

3) Bulk $Al_{86}Ni_7Y_{4.5}Co_1La_{1.5}$ nanostructured materials are fabricated by CIP and VHE with high energy ball milled powder as starting materials. A compressive strength of 650 MPa is achieved in the bulk $Al_{86}Ni_7Y_{4.5}Co_1La_{1.5}$ nanostructured samples.

References

[1] HE Y, POON S J, SHIFLET G J. Synthesis and microstructural evolution of Al−Ni−Fe−Gd metallic glass by mechanical alloying [J]. Science, 1988, 241: 1640−1642.

[2] INOUE A. Bulk amorphous alloys [J]. Progress Materials Science, 1988, 43: 365−520.

[3] KIM Y H, INOUE A, MASUMOTO T. Elevated-temperature strength of an $Al_{88}Ni_9Ce_2Fe_1$ amorphous alloy containing nanoscale fcc-Al particles [J]. Materials Transactions JIM, 1992, 33: 669−674.

[4] SUN Xian-zhong, PAN Hong-ge, GAO Ming-xia. Cycling stability of La−Mg−Ni−Co type hydride electrode with Al [J]. Transactions of Nonferrous Metals Society of China, 2006, 16(1): 8−12.

[5] ZHONG Z C, JIANG X Y, GREER A L. Nanocrystallization in Al-based amorphous alloys [J]. Philosophical Magazane B, 1997, 76(4): 505−510.

[6] TSAI A P , KAMIYAMA T, KAWAMURA Y. Formation and precipitation mechanism of nanoscale Al particles in Al−Ni base amorphous alloys [J]. Acta Materialia, 1997, 45(4): 1477−1487.

[7] GLORIANT T, PING D H, HONO K, GREER A L, BARÓ M D. Nanostructured $Al_{88}Ni_4Sm_8$ alloys investigated by transmission electron and field-ion microscopies [J]. Materials Science and Engineering A, 2001, 304: 315−320.

[8] INOUE A, KIMURA H. High-strength aluminum alloys containing nanoquasicrystalline particles [J]. Material Science and Engineering A, 2000, 286(1): 1−10.

[9] INOUE A , SOBU S, LOUZGUINE D V, KIMURA H, SASAMORI K. Ultrahigh strength Al-based amorphous alloys containing Sc [J]. Materials Research, 2004, 19: 1539−1543.

[10] LEE Kwang-Seok, KWON Yong-Nam. Solid-state bonding between Al and Cu by vacuum hot pressing [J]. Transactions of Nonferrous Metals Society of China, 2013, 23(2): 341−346.
[11] PORTIER R A, OCHIN P, PASKO A, MONASTYRSKY G E. Spark plasma sintering of Cu−Al−Ni shape memory alloy [J]. Journal of Alloys and Compounds, 2013, 577(1): s472−s477.
[12] KAWAMURA Y, SHIBATA T, INOUE A, et al. Workability of the supercooled liquid in the $Zr_{65}Al_{10}Ni_{10}Cu_{15}$ bulk metallic glass [J]. Acta Materialia, 1998, 46(1): 253−263.
[13] YE L L, LIU Z G, RAVIPRASAD K, QUAN M X, UMEMOTO M. Consolidation of MA amorphous NiTi powder by spark plasma sintering [J]. Material Science and Engineering A, 1998, 241(1): 290−293.
[14] SORDELET D J, ROZHKOVA E, BESSER M F, KRAMER M J. Consolidation of gas atomized $Cu_{47}Ti_{34}Zr_{11}Ni_8$ amorphous powder [J]. Journal of Non-crystalline Solids, 2003, 317(1): 137−143.
[15] CHIANG C H, TSAO C Y A. Si coarsening of spray-formed high loading hypereutectic Al−Si alloys in the semisolid state mate [J]. Material Science and Engineering A, 2005, 396: 263−270.
[16] ALLIMANT A, PLANCHE M P, BAILLY Y, DEMBINSKI L, CODDET C. Progress in gas atomization of liquid metals by means of a De Laval nozzle [J]. Powder Technology, 2009, 190: 79−83.
[17] BAO C M, DAHLBORG U , ADKINS N, CALVO-DAHLBORG M. Structural characterization of Al−Ni powders produced by gas atomization [J]. Journal of Alloys and Compounds, 2009, 481: 199−206.
[18] LIU D, ZHAO J, YE H. Modeling of the solidification of gas-atomized alloy droplets during spray forming [J]. Material Science and Engineering A, 2004, 372: 229−234.
[19] LEE T H, KAWAMURA Y, INOUE A, CHO S S. Mechanical properties of rapidly solidified Al−Si−Ni−Ce P/M alloys [J]. Script Materialia, 1997, 36: 475−480.

机械合金化和烧结工艺对 Al−Ni−Y−Co−La 合金显微组织及力学性能的影响

原燕波[1]，王志伟[1]，郑瑞晓[1]，郝晓宁[1]，Kei AMEYAMA[2]，马朝利[1]

1. 北京航空航天大学 材料科学与工程学院，空天先进材料与服役教育部重点实验室，北京 100191；
2. Department of Mechanical Engineering, Faculty of Science and Engineering, Ritsumeikan University, 1-1-1Nojihigashi, Kusatsu, Shiga 525-8577, Japan

摘 要：通过气雾化方法制备 $Al_{86}Ni_7Y_{4.5}Co_1La_{1.5}$(摩尔分数，%)合金粉末。首先，将粉末进行不同时间的球磨，然后在不同的烧结温度及保压时间等条件下对粉末分别进行热压烧结和放电等离子烧结。通过 X 射线衍射仪(XRD)，扫描电镜(SEM)以及透射电镜(TEM)对粉末和块体材料的显微组织和形貌进行表征。结果表明：在特定球磨参数下球磨 100 h 以上可以产生非晶，而且通过放电等离子烧结可以得到非晶/纳米晶块体材料，然而这种材料的相对密度较低。通过热压烧结可制备抗压强度为 650 MPa 的 $Al_{86}Ni_7Y_{4.5}Co_1La_{1.5}$ 纳米块体材料。

关键词：机械合金化；铝合金；纳米晶；非晶；放电等离子烧结；热挤压

(Edited by Chao WANG)